Contents lists available at ScienceDirect

Transactions of Nonferrous Metals Society of China

36(2026) 988−999

www.tnmsc.cn

Simulation prediction and experimental study of phase equilibrium for Ag−Cu and Ag−Sb binary alloys in vacuum distillation

Qing-song LI [a,b,c], Bin YANG [a,b,c,d], Yang TIAN [a,b,c,d,*], Bao-qiang XU [a,b,c,d], Wen-long JIANG [a,b,c,d], Yuan GAO [a,b,c], Zong-kui JIANG [a,b,c]

[a] Key Laboratory for Nonferrous Vacuum Metallurgy of Yunnan Province, Kunming University of Science and Technology, Kunming 650093, China;

[b] National Engineering Research Center of Vacuum Metallurgy, Kunming University of Science and Technology, Kunming 650093, China;

[c] Faculty of Metallurgical and Energy Engineering, Kunming University of Science and Technology, Kunming 650093, China;

[d] State Key Laboratory of Complex Nonferrous Metal Resources Clean Utilization, Kunming University of Science and Technology, Kunming 650093, China

Abstract: The modified molecular interaction volume model (M-MIVM) was used to calculate the activity values and their deviations from experimental data for Ag−Cu and Ag−Sb binary alloys. Subsequently, theoretical vapor−liquid equilibrium phase diagrams (T−x−y and p−x−y) were plotted via combining M-MIVM and vacuum theory. The vapor−liquid phase equilibrium (VLE) experiments were conducted on the Ag−Cu alloy at 1500−1560 K and 10−15 Pa and Ag−Sb alloys at 950−1350 K and 10 Pa. The results showed that the average relative deviation and average standard deviation of activity were lower than 5% and 0.02, respectively. A comparison of theoretical and experiment results for VLE revealed that the simulated data on the T−x−y diagram were well consistent with experimental values. Therefore, the VLE phase diagrams can serve as a guide in vacuum separation experiments and industrial production for Ag−Cu and Ag−Sb binary alloys.

Keywords: Ag−Cu binary alloy; Ag−Sb binary alloy; modified molecular interaction volume model (M-MIVM); vapor−liquid phase equilibrium; activity

1 Introduction

Silver, a white metal, boasts unique properties such as corrosion resistance [1] and stability [2]. It finds application in various fields, primarily in the electronic industry [3], photography [4], aerospace engines and so on. Silver also plays a significant role in the financial sector [5] and has a rich history as currency, spanning millennia. It continues to hold value as a collectible currency, while also being extensively consumed in the creation of female ornaments [6]. Moreover, silver is widely employed in high technology, e.g., as a contact in chips and fuses due to its excellent conductivity [7,8], good flexibility [9], and high performance. Meanwhile, it is one of primary metals applied in medicine [10]. In ancient times, silverware was used to detect the presence of poisons in food. This is because the arsenic trioxide contains sulfur and its complexes that form black compounds with silver. In 2022, the global demand for silver reached 38000 t, but the real production was limited to 26000 t, indicating an oversupply situation [11]. Therefore, it is urgent to

Corresponding author: *Yang TIAN, Tel: +86-13888805314, E-mail: emontian@hotmail.com

https://doi.org/10.1016/S1003-6326(25)67011-7

Received 30 May 2024; accepted 7 March 2025

search for an efficient way of producing silver so as to fulfill societal needs.

The vacuum approach with advantages of short flow [12], high efficiency [13] and environmental friendliness [14] is extensively utilized in the extraction of precious metals, including silver and gold, from heavy colored anodic sludge [15,16]. When designing vacuum distillation experiments or industrial production routes for an alloy, the reliable VLE diagrams are essential for estimating the temperature and separation efficiency during alloy separation [17]. Therefore, adequate VLE data are crucial. They provide an intuitive and convenient approach for analyzing distillation and other vapor−liquid separation processes, making them widely applicable in the chemical industry [18]. However, the industrial alloy separation primarily involves multiple components, for which experimental data are often scarce and challenging to obtain through experimentation. Thus, the theoretical prediction [19,20] is an efficient method for acquiring the thermodynamic properties of multivariate alloys. Additionally, KONG et al [21] established a VLE prediction model by combining activity and vacuum theories. Since recently, the modified molecular interaction volume model (M-MIVM) has been applied to predicting the activity and VLE values of Ag-based and In-based alloy systems [22,23]. The M-MIVM is an outstanding thermodynamic model, maintaining the superb forecasting capability not only for symmetric systems, but also for asymmetric ones [24]. For the Ag−Cu and Ag−Sb binary alloys, YOU et al [25,26] calculated the activity of each group element using M-MIVM. However, the simulative studies and experiments on VLE have not been reported so far.

In view of the above, this work aimed to assess the activity and activity coefficients of Ag−Cu and Ag−Sb binary alloys via M-MIVM. The predicted results were compared with experimental data from Refs. [27,28]. The VLE theoretical values for Ag−Cu and Ag−Sb binary alloys were afterward calculated by combining the M-MIVM and vacuum theory. Finally, the VLE experiments were conducted for Ag−Cu and Ag−Sb binary alloys, and the experimental phase diagrams were compared with theoretical VLE data. Thus, the reliability of VLE phase diagrams for Ag−Cu and Ag−Sb binary alloys was verified for the first time, offering reliable guidance for separating these alloys in both experimental and industrial vacuum distillation processes.

2 Experimental

2.1 Materials

The original materials comprised Ag powders (Mengzi Mining and Metallurgy Company), Cu grains (Yunnan Precious Metal New Material Holding Group Company), and Sb grains (Aladdin website). These materials were chemically analyzed in accordance with GB/T 4135—2016, GB/T 467—2010, and GB/T 1599—2014 standards. The purities of Ag, Cu, and Sb metals were greater than 99.99%, 99.99%, and 99.9%, respectively. The information concerning Ag, Cu, and Sb metals is listed in Table 1.

2.2 Devices and procedures

The experiments conducted in this study took two main contents, as illustrated in Fig. 1. Initially, various original materials were mixed in specific ratios and formulated together using a resistance furnace. Subsequently, alloy samples underwent vacuum distillation experiments to separate volatiles from residues.

The alloy preparation is depicted in Fig. 2(a). It primarily involves a heating device-resistance furnace, a corundum crucible with original materials or an alloy sample, a quartz tube, a resistance furnace controller, an argon cylinder, a vacuum pump, and a quenching device, which is a bucket filled with water. Additionally, a pressure vacuum indicator was used to assess the degree of washing and exchange. The specific operational steps are as follows.

Table 1 Brand and purity of Ag, Cu, and Sb metals

Metal	Purity/wt.%	National standard	Brand
Ag	≥99.99	GB/T 4135—2016	Mengzi Mining and Metallurgy Company
Cu	≥99.99	GB/T 467—2010	Yunnan Precious Metal New Material Holding Group Company
Sb	≥99.90	GB/T 1599—2014	Aladdin website

Fig. 1 Experimental procedure including original materials, alloy samples, and products after vacuum distillation

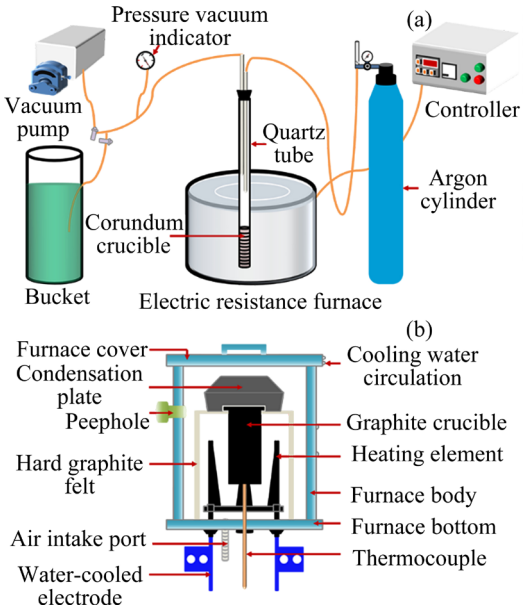

Fig. 2 Experimental device: (a) Flowchart of alloy formulation; (b) Diagram of vacuum furnace structure

Firstly, the original materials required for different ratio alloys were accurately weighed and thoroughly mixed. Secondly, the phase diagram of an alloy was examined to determine the fusion temperature for preparing the alloy sample. Thirdly, the quartz tube containing original materials (or alloy samples) was evacuated using a vacuum pump and then filled with argon gas to exclude the atmosphere. This stage was repeated 3−5 times and was followed by continuous filling with argon gas so as to ensure the sample will not oxidize during the thermal insulation. After the first thermal insulation for 2 h at a certain fusion temperature, the quartz tube with the alloy samples was immediately quenched in a bucket without stopping the argon gas flow for 20−40 min. The last two steps were iterated until the alloy sample was fully melted and thoroughly mixed.

In this study, the melting temperatures of Ag−Cu (m_{Ag}:m_{Cu}=9:4) and Ag−Sb (m_{Ag}:m_{Sb}=5.6:7.4) binary alloys (each with a mass of 13 g) were determined to be 1123 and 823 K, respectively, as per the corresponding phase diagrams [29,30]. Moreover, the argon gas (99.99% purity) was fed at rate of 0.2−0.3 L/min. The Ag−Cu and Ag−Sb binary alloy samples are shown in Fig. 1, whose mass loss did not exceed 5%.

Figure 2(b) depicts the schematic diagram of a vacuum furnace, capable of reaching pressures up to 10 Pa. To begin with, a high-purity graphite crucible containing the alloy sample was positioned at the center of the graphite heaters. The condensation plate and furnace cover were then accordingly applied. The cooling water circulation was turned on to prevent overheating of the furnace. When the pressure within the vacuum furnace reached 10−20 Pa, the heating power on the control cabinet was adjusted to raise the temperature. The holding was initiated as soon as the desired temperature and pressure conditions were met. After heat preservation, the heating power valve was regulated to zero. Once the temperature fell below 60−90 °C, the vacuum pump was turned off and the furnace cover was opened. Finally, volatiles and residues were taken off for weighing and preparing samples for subsequent analysis.

3 Model

3.1 M-MIVM

The M-MIVM was developed by DAI and TAO [31] by combining the MIVM with Scott's two-fluid theory and Scatchard−Hildebrand theory. This enabled to separate the enthalpy and entropy parameters within the MIVM based on the radial distribution theory, freely switching between enthalpy and entropy dominant roles in alloys. The Scatchard−Hildebrand theory was subsequently integrated to augment the complexity of the enthalpy expression. The molar excess Gibbs energy (G_m^E) for a binary alloy is expressed as follows:

$$\frac{G_m^E}{RT}=-x_i\ln\left(x_i+x_j\frac{V_{mj}}{V_{mi}}B_{ji}\right)-x_j\ln\left(x_j+x_j\frac{V_{mi}}{V_{mj}}B_{ij}\right)+$$
$$x_ix_j\left(\frac{A_{ji}}{x_i+x_i\dfrac{V_{mj}}{V_{mi}}B_{ij}}+\frac{A_{ij}}{x_j+x_j\dfrac{V_{mi}}{V_{mj}}B_{ji}}\right) \quad (1)$$

$$A_{ij}=K'C_j^0(\varepsilon_{ij}-\varepsilon_{jj}) \tag{2}$$

Then,

$$K'=\frac{3K}{k} \tag{3}$$

$$B_{ij}=\frac{P_{ij}}{P_{jj}} \tag{4}$$

where A_{ij} and B_{ij} are the volume and energy parameters defined by Eqs. (2) and (4), respectively; C_j^0 is a proportional constant; ε_{ij} is the potential energy of the molecular pair between i and j; K is a universal constant independent of the molecular nature; k is the Boltzmann constant; P_{ij} is the probability of the molecule i to arise in the first coordination layer of the nuclear molecule j; V_{mi} is the molar volume at a specific temperature, which can be found in Table 2.

Table 2 Data on Ag, Cu, and Sb metals required for M-MIVM [32]

Metal	$V_{mi}/(10^{-6}\mathrm{m^3\cdot mol^{-1}})$	T_{mi}/K
Ag	$11.64(1+0.98\times10^{-4}(T-T_{mi}))$	1234
Cu	$7.99(1+1.00\times10^{-4}(T-T_{mi}))$	1356
Sb	$18.87(1+1.3\times10^{-4}(T-T_{mi}))$	904

Since the volume parameter B_{ij} is temperature-dependent, then the value of B_{ij0} at an arbitrary temperature T_0 can be obtained from Eq. (5). The energy parameter A_{ij} is also closely related to the temperature according to Eq. (6).

$$B_{ij0}=\exp\left(\frac{T}{T_0}\ln B_{ij}\right) \tag{5}$$

$$A_{ij0}=\frac{T}{T_0}A_{ij} \tag{6}$$

Simultaneously, the activity coefficient of the component i (γ_i) in binary systems can be expressed as

$$\ln\gamma_i=-\ln\left(x_i+\frac{V_{mj}}{V_{mi}}B_{ji}x_j\right)-x_ix_j\left[\frac{1-\frac{V_{mj}}{V_{mi}}B_{ji}}{x_i+\frac{V_{mj}}{V_{mi}}B_{ji}x_j}\right]-x_j^2\left[\frac{\frac{V_{mi}}{V_{mj}}B_{ij}-1}{x_j+\frac{V_{mi}}{V_{mj}}B_{ij}x_i}\right]+x_j^2\left[\frac{A_{ji}}{x_i+\frac{V_{mj}}{V_{mi}}B_{ji}x_j}+\frac{A_{ij}}{x_j+\frac{V_{mi}}{V_{mj}}B_{ij}x_i}\right]-x_ix_j^2\left[\frac{A_{ji}(1-\frac{V_{mj}}{V_{mi}}B_{ji})}{(x_i+\frac{V_{mj}}{V_{mi}}B_{ji}x_i)^2}+\frac{A_{ij}(\frac{V_{mi}}{V_{mj}}B_{ij}-1)}{(x_j+\frac{V_{mi}}{V_{mj}}B_{ij})^2}\right]^2 \tag{7}$$

3.2 Vapor−liquid phase equilibrium

When using vacuum technology to separate alloys, the quantitative analysis of the alloy component distribution in vapor and liquid phases can be carried out through the VLE phase diagrams, namely T–x–y and p–x–y diagrams [21]. The key equations for obtaining VLE phase diagram data in binary alloys are as follows:

$$y_i=\gamma_ix_ip_i^*/p \tag{8}$$

$$p=p_i^*\gamma_ix_i+p_j^*\gamma_jx_j \tag{9}$$

where x_i and y_i represent the content of the component i in liquid and vapor phases, respectively; p denotes the total system pressure; p_i^* is the saturation vapor pressure of the component i, which is calculated from the equation below:

$$\lg p^*=A/T+B\lg T+CT+D \tag{10}$$

where A, B, C, and D represent evaporation constants, whose values for Ag, Cu, and Sb are given in Table 3.

Table 3 Evaporation constants of Ag, Cu, and Sb metals [33]

Metal	A	B	C	D	T/K
Ag	−14400.00	−0.85	0.00	11.70	1234−2420
Cu	−17520.00	−1.21	0.00	13.21	1356−2843
Sb	−6500.00	0.00	0.00	6.37	904−1948

Figure 3 depicts the algorithm enabling to calculate the VLE phase equilibrium for binary alloys. For the T–x–y diagram, a series of x_i, system pressure p, and initial temperature T are first set. Then, the activity coefficient γ_i and saturated vapor pressure p_i^* of Ag, Cu, and Sb are calculated at temperature T. After that, the obtained values are substituted into Eq. (9) to establish the system pressure p'. Once the condition of $|p'-p|/p\leq0.01\%$ is

satisfied, the temperature T is defined. Finally, the values p, γ_i, p_i^*, and x_i are substituted into Eq. (8) to obtain y_i. The same procedure is executed for the p–x–y diagram and relatively simple. Figures 7 and 8 depict the T–x–y and p–x–y diagrams for Ag–Cu and Ag–Sb binary alloys, respectively.

4 Result and discussion

4.1 Activity calculation

The energy parameters B_{ij} and B_{ji} in the M-MIVM can be obtained by substituting the experimentally found infinite activity coefficients into the Newton formula. For the Ag−Cu binary alloy at 1423 K, these values are 0.36 and 0.555, while for the Ag−Sb binary alloy at 1250 K, they are 1.922, and 7.013. Other important parameters, A_{ij} and A_{ji}, are 0.032 and −0.092 for the Ag−Cu binary alloy at 1423 K, while being 1.594 and 6.675 for the Ag−Sb binary alloy at 1250 K [25,26]. Tables 4 and 5 list the predicted activities for components i and j of Ag−Cu and Ag−Sb binary alloys, respectively. It is evident from Fig. 4 that the M-MIVM-predicted activity data align with the experimental values for both alloys. To evaluate the accuracy of the predictions, the average relative deviation S_i and the average standard deviation S_i^* were also calculated according to the following equations [23]:

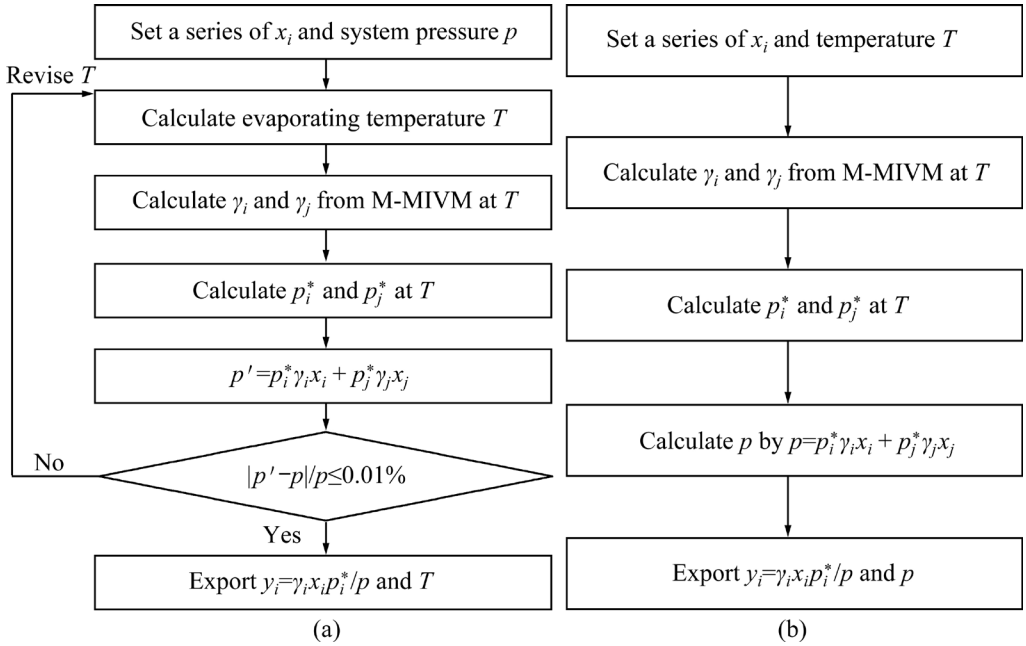

Fig. 3 Flowchart with calculation algorithm of VLE phase diagrams: (a) T–x–y; (b) p–x–y

Table 4 Predictive and experimental data on activity (a) and activity coefficient (γ) of Ag−Cu binary alloy at 1423 K [28]

x_{Ag}	$a_{Ag,exp}$	$a_{Cu,exp}$	$a_{Ag,pre}$	$a_{Cu,pre}$	$\gamma_{Ag,exp}$	$\gamma_{Cu,exp}$	$\gamma_{Ag,pre}$	$\gamma_{Cu,pre}$
0.1	0.26600	0.91200	0.26583	0.91211	2.65560	1.01300	2.65831	1.01345
0.2	0.43100	0.84100	0.42772	0.84239	2.15400	1.05100	2.13859	1.05298
0.3	0.53700	0.78200	0.53414	0.78344	1.79000	1.11800	1.78045	1.11919
0.4	0.61000	0.73100	0.61083	0.72933	1.52500	1.21800	1.52707	1.21554
0.5	0.66700	0.67900	0.67223	0.67449	1.33400	1.35900	1.34447	1.34898
0.6	0.72200	0.61600	0.72720	0.61253	1.20300	1.54100	1.21201	1.53132
0.7	0.77900	0.53500	0.78194	0.53461	1.11300	1.78200	1.11706	1.78202
0.8	0.84100	0.42200	0.84169	0.42669	1.05200	2.11200	1.05211	2.13343
0.9	0.91200	0.26000	0.91199	0.26415	1.01400	2.60000	1.01333	2.64151
±S/%			0.38436	0.51095				
±S^*			0.00304	0.00295				

Table 5 Predictive and experimental data on activity and activity coefficient of Ag−Sb binary alloy at 1250 K [27]

x_{Ag}	$a_{Ag,exp}$	$a_{Sb,exp}$	$a_{Ag,pre}$	$a_{Sb,pre}$	$\gamma_{Ag,exp}$	$\gamma_{Sb,exp}$	$\gamma_{Ag,pre}$	$\gamma_{Sb,pre}$
0.1	0.05800	0.90200	0.05563	0.92959	0.57900	1.00300	0.55629	1.03288
0.2	0.10800	0.81200	0.10234	0.82126	0.54100	1.01500	0.51170	1.02658
0.3	0.15700	0.71800	0.14809	0.71484	0.52300	1.02600	0.49362	1.02120
0.4	0.20900	0.61500	0.19937	0.60402	0.52200	1.02600	0.49842	1.00671
0.5	0.26500	0.50700	0.26292	0.49056	0.52900	1.01400	0.52585	0.98111
0.6	0.32400	0.39500	0.34721	0.34821	0.54000	0.98800	0.57868	0.87053
0.7	0.46200	0.20300	0.46366	0.20216	0.65900	0.67600	0.66237	0.67386
0.8	0.65300	0.07100	0.62618	0.08067	0.81600	0.35400	0.78272	0.40332
0.9	0.85300	0.01510	0.83633	0.01473	0.94800	0.15100	0.92926	0.14728
$\pm S$/%			3.77584	4.22260				
$\pm S^*$			0.01396	0.01981				

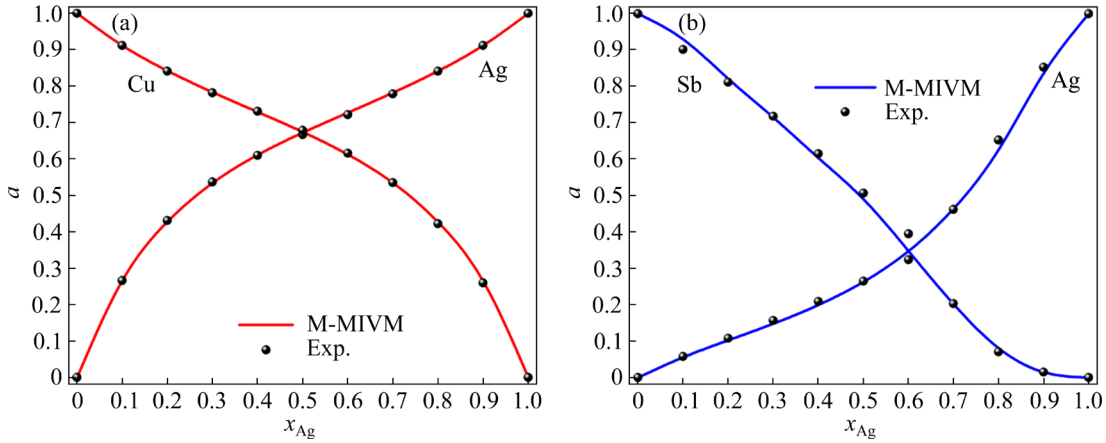

Fig. 4 Comparison between predicted and experimental data on activity [27,28]: (a) Ag−Cu binary alloy (1423 K); (b) Ag−Sb binary alloy (1250 K)

$$S_i = \pm \frac{100}{n} \sum_{i=1}^{n} \left| \frac{a_{i,pre} - a_{i,exp}}{a_{i,exp}} \right| \quad (11)$$

$$S_i^* = \pm \left[\frac{1}{n} \sum_{i=1}^{n} (a_{i,pre} - a_{i,exp})^2 \right]^{1/2} \quad (12)$$

where $a_{i,pre}$ and $a_{i,exp}$ are the predicted and experimental activity values, respectively; n is the number of comparison data. The respective values were found to be less than 5% and 0.02, respectively.

4.2 VLE

4.2.1 Formulation of alloys

The chemical composition of alloy samples was analyzed and compared to the designed ratios. The results are displayed in Table 6, indicating that the mass fractions of components detected in the Ag−Cu and Ag−Sb binary alloys were in accordance with theoretical values, which meet the experimental design requirements. Additionally, the SEM−ESD was employed to establish whether the components in these alloys were uniformly distributed, and the corresponding images are illustrated in Fig. 5. The plots reveal that each element in both the Ag−Cu and Ag−Sb binary alloys is evenly distributed, allowing any errors in the alloy samples to be neglected for subsequent vacuum distillation experiments in the present research.

Table 6 Composition of Ag−Cu and Ag−Sb binary alloy samples (wt.%)

System (i–j)	i	j	i^*	j^*
Ag−Cu	69.23	30.77	69.19	30.81
Ag−Sb	43.08	56.92	45.53	54.47

* Chemical testing result

4.2.2 Determination of equilibrium time

A system is assumed to approach an equilibrium state when the volatility of the sample tends to stabilize [34]. Consequently, the corresponding distillation time can be regarded as the equilibrium time. The volatility (v) is obtained by

$$v=\frac{m_{\text{Total}}-m_{\text{Residue}}}{m_{\text{Total}}}\times 100\% \tag{13}$$

where m_{Total} and m_{Residue} denote the mass of alloy samples and residues after vacuum distillation experiments, respectively.

Moreover, the thermal movement of molecules is positively correlated with temperature, meaning that higher temperatures enable to faster attain equilibrium. Therefore, the experimental investigation of equilibrium time at the lowest temperature was carried out prior to vapor−liquid phase equilibrium experiments.

Figure 6 displays the equilibrium time investigation results for Ag−Cu binary alloy at 1500 K and 10−15 Pa and Ag−Sb binary alloy at 950 K and 10 Pa. It is clear that the Ag−Cu binary alloy tends to stabilize after 4 h, while the volatility reaches its peak at 5.3 h. Similarly, the Ag−Sb binary alloy has a steady tendency when the distillation time is incrementally extended every half hour after 8.3 h. Furthermore, when the holding time reaches 9.3 h, the volatility of Ag−Sb binary alloy enriches its maximum value. Consequently, the equilibrium time is determined to be 5.3 h for the Ag−Cu binary alloy at 1500 K and 9.3 h for the Ag−Sb binary alloy at 950 K. Although the high temperature should theoretically reduce the equilibrium time, the temperature difference was set at 20 K for the Ag−Cu binary alloy, thus the equilibrium time at other temperatures also remained 5.3 h. This ensures that the system has the adequate time to reach an equilibrium state. For the Ag−Sb binary alloy, Sb compounds could influence the experimental outcomes.

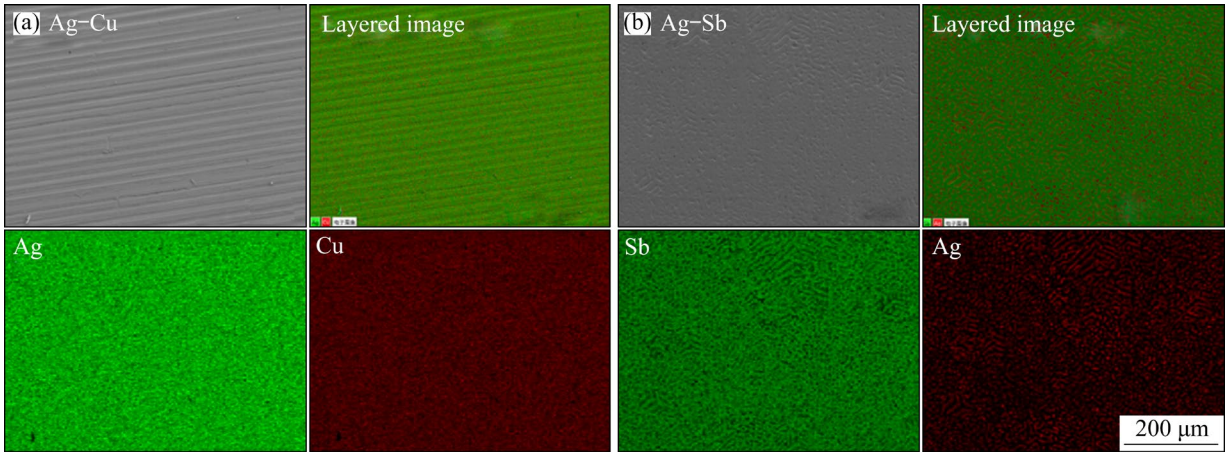

Fig. 5 SEM−EDS results of alloys: (a) Ag−Cu binary alloy; (b) Ag−Sb binary alloy

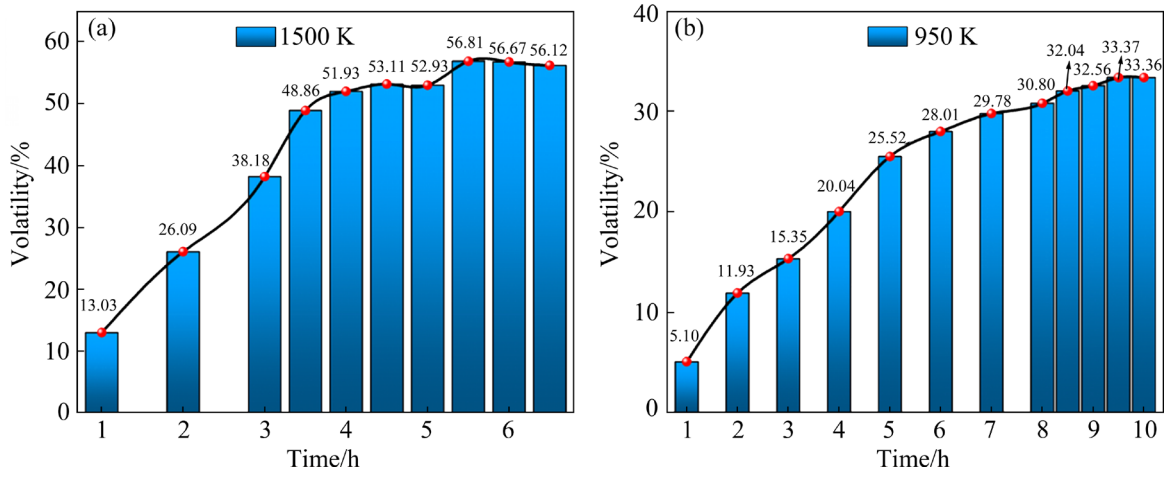

Fig. 6 Relationship between volatility and distillation time: (a) Ag−Cu binary alloy at 1500 K; (b) Ag−Sb binary alloy at 950 K

In this respect, the holding time is standardized at 9.3 h for VLE experiments at high temperatures to minimize experimentally induced errors and ensure data accuracy. The VLE experimental conditions for Ag−Cu and Ag−Sb binary alloys are listed in Tables 7 and 8.

4.2.3 Comparison between theoretical and experimental values of VLE

Following the equilibrium time results, VLE experiments were conducted on Ag−Cu and Ag−Sb binary alloys, and the experimental data are presented in Tables 7 and 8, respectively. Figures 7 and 8 display the respective experimental and theoretical values. The points on the plots represent the VLE experimental data obtained through the vacuum distillation, while the curves depict the VLE forecast data calculated using M-MIVM and vacuum theory.

As seen from Fig. 7, the experimental VLE data and the predicted VLE phase diagram (T–x–y) follow the same trend with the temperature change and basically coincide with each other for Ag−Cu

Table 7 VLE-calculated and experimental data along with experimental conditions in Ag−Cu binary alloy

No	T/K	p/Pa	Time/h	$x_{Ag,exp}$	$y_{Ag,exp}$	$y_{Ag,cal}$	Δy_{max}	$y_{(MAD)}$
1	1500	10−15	5.3	0.20404	0.92746	0.96262−0.96593	0.03847	3.45515−4.11147
2	1520	10−15	5.3	0.11926	0.90924	0.93917−0.94456	0.03532	
3	1540	10−15	5.3	0.09409	0.87169	0.92377−0.93045	0.05876	
4	1560	10−15	5.3	0.05367	0.84790	0.86894−0.87982	0.03192	

$\Delta y_{max}=\max|y_{i,exp}-y_{i,cal}|$

Table 8 VLE-calculated and experimental data along with experimental conditions in Ag−Sb binary alloy

No	T/K	p/Pa	Time/h	$x_{Ag,exp}$	$y_{Sb,exp}$	$y_{Sb,cal}$	Δy	$y_{(MAD)}$
1	950	10	9.3	0.65476	0.99593	1.00000	0.00407	
2	1000	10	9.3	0.67993	0.97261	1.00000	0.02738	
3	1050	10	9.3	0.71279	0.98585	0.99999	0.01414	
4	1100	10	9.3	0.73287	0.97436	0.99998	0.02562	
5	1150	10	9.3	0.75931	0.98773	0.99996	0.01223	4.94897
6	1200	10	9.3	0.78029	0.97185	0.99993	0.02810	
7	1250	10	9.3	0.80770	0.94080	0.99981	0.05901	
8	1300	10	9.3	0.82475	0.93280	0.99965	0.06685	
9	1350	10	9.3	0.83667	0.79141	0.99944	0.20803	

$\Delta y=|y_{i,exp}-y_{i,cal}|$

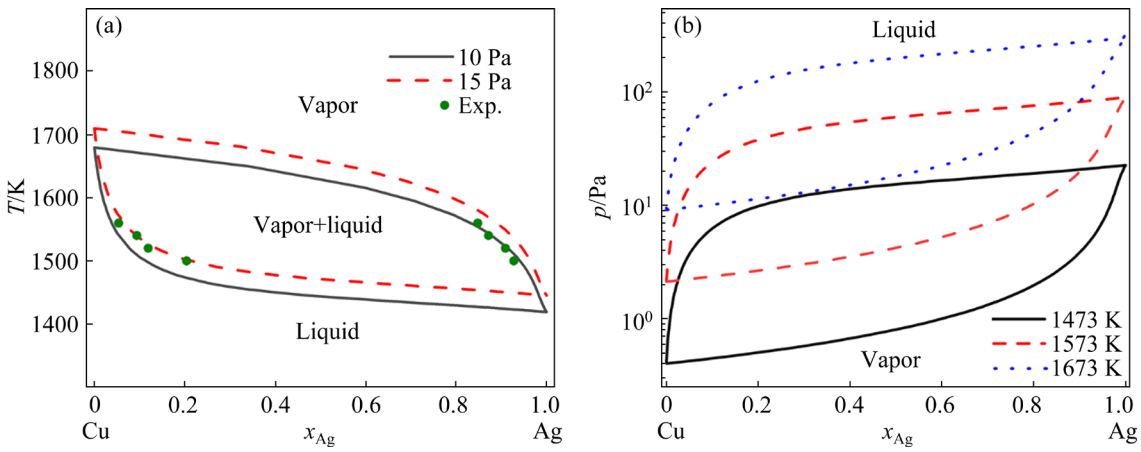

Fig. 7 VLE phase diagram of Ag−Cu binary alloy: (a) T–x–y (10−15 Pa); (b) p–x–y (1473−1673 K)

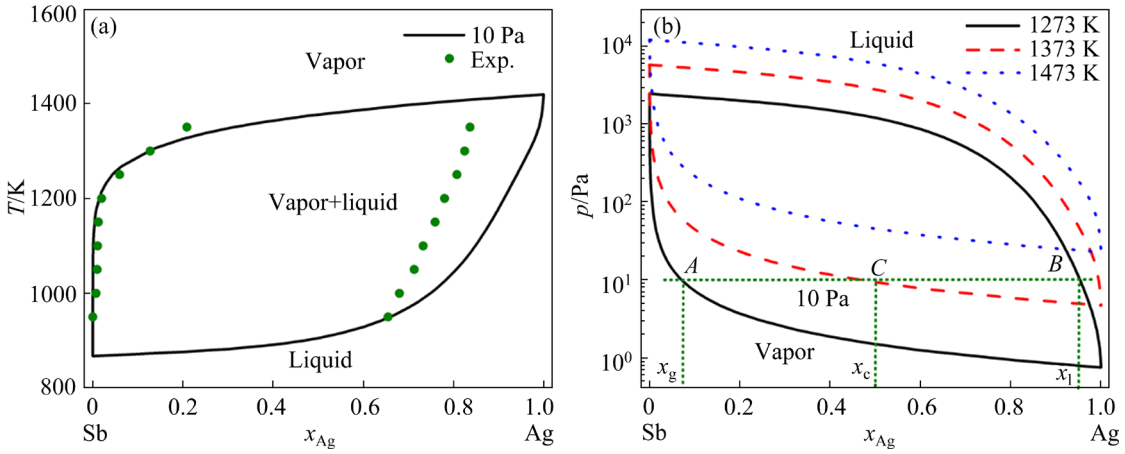

Fig. 8 VLE phase diagram of Ag−Sb binary alloy: (a) *T*–*x*–*y* (10 Pa); (b) *p*–*x*–*y* (1273−1473 K)

binary alloy. In addition, Table 7 reveals the minor deviation between theoretical and experimental data for the Ag vapor phase of Ag−Cu binary alloys at temperatures of 1500, 1520, 1540, and 1560 K. To assess the data reliability, the parameter $y_{(\mathrm{MAD})}$ was calculated as follows [35]:

$$y_{(\mathrm{MAD})}=\frac{1}{N}\sum_{i=1}^{N}100\,|\,y_{i,\mathrm{exp}}-y_{i,\mathrm{cal}}\,| \tag{14}$$

where N denotes the number of experiments; $y_{i,\mathrm{exp}}$ and $y_{i,\mathrm{cal}}$ are the VLE experimental data and the theoretical value for the group element i, respectively. According to the estimation, $y_{(\mathrm{MAD})}>1$, indicating poor reliability of experimental data [35]. This experimental deviation mainly originates from the non-ideal experimental conditions for alloy separation, equipment limitations, and potential inaccuracies in the chemical analysis of experimental results.

As illustrated in Fig. 8, the temperature dependence of experimental data is in accordance with the *T*–*x*–*y* diagram for the Ag−Sb binary alloy. The experimental values of Ag content in the vapor phase closely match the theoretical values, thereby validating the reliability of the VLE prediction based on the M-MIVM. In other words, this good alignment confirms the dependability of the M-MIVM. However, there is a discrepancy between the theoretical and experimental Ag contents in the liquid phase, which stems from the two aspects. One relies on the experimental variables, including experimental conditions of non-ideal equilibrium states, potential mass losses, or the inability of metal vapor to return to the liquid phase after condensation. Nonetheless, these factors could be ignored in this project. It is believed that the main reason for the deviation in the Ag−Sb binary alloy in this study originates from the issues within the system. The Ag−Sb binary alloy is a negative deviation system, which displays a negative slop of the curve, making it challenging to separate constituents via the vacuum method due to the strong interaction between Sb and Ag. In other words, the interplay between components within the negative deviation system inhibits their separation from an activity perspective, whereas the interaction between components in positive deviation systems promotes the component separation [36]. Combining this conclusion with Fig. 4, it becomes apparent that the Ag−Sb binary alloy is indeed a negative deviation system, while the Ag−Cu binary alloy is a positive deviation system. Thus, there is a substantial deviation between theoretical and experimental VLE data for the Ag−Sb binary alloy. Besides that, the X-ray diffraction (XRD) analysis of the residues within the Ag−Sb binary alloy (Fig. 9(a)) revealed that the residue phases also contained the Ag_3Sb moieties in addition to Sb, confirming the cause of the deviation. Meanwhile, Fig. 9(b) shows that no Ag−Cu alloy compounds were detected in the residues of the Ag−Cu binary alloy after vacuum distillation. Therefore, separating Ag and Sb through a single vacuum distillation technology is not feasible. However, multiple separations of this alloy may be guided by the VLE phase diagrams.

Therefore, the VLE results based on the M-MIVM are reliable and reaffirm the dependability of the M-MIVM in this work. The closer alignment between experimental points and theoretical curves

indicates that VLE phase diagrams (T–x–y or p–x–y) can effectively guide the vacuum separation process and predict separation conditions for Ag−Cu and Ag−Sb binary alloys. Specifically, for the Ag−Sb binary alloy at 1273 K and 10 Pa, a 100 g-sample with 50% Ag should theoretically yield 49.20 g of residues and 50.80 g of distillate, which follows from the leverage theorem ($x_{AC}w_g=x_{CB}w_l$ [37]). The respective data are displayed in Fig. 8(b). Meanwhile, the optimal separation temperature can be determined from the T–x–y diagram. In the case of the Ag−Sb binary alloy under 10 Pa, temperatures below 1025.14 K enable to obtain distillate products with Sb content exceeding 99.99%, while temperatures above 1417.91 K may yield distillate products containing more than 99% Ag.

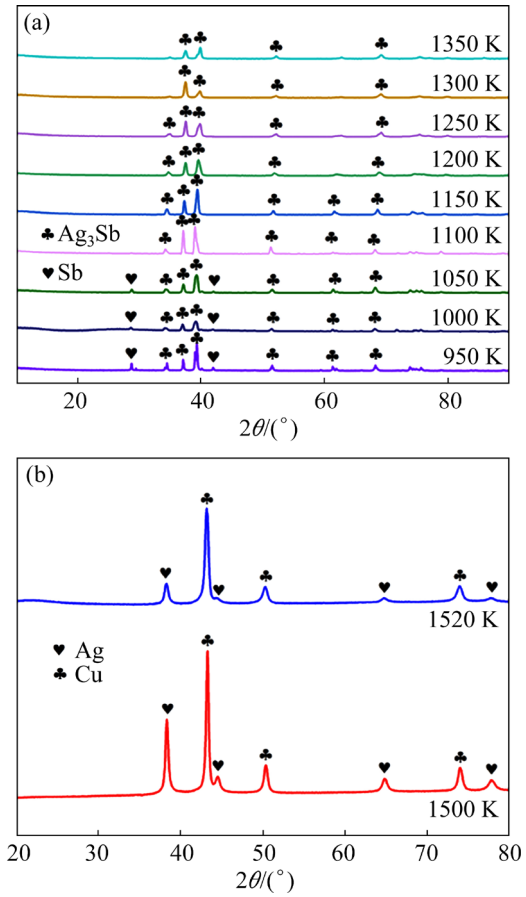

Fig. 9 XRD patterns of residues: (a) Ag−Sb alloy at 950−1350 K; (b) Ag−Cu alloy at 1500−1520 K

5 Conclusions

(1) The activity and activity coefficients for Ag−Cu and Ag−Sb binary alloys were calculated using the M-MIVM across the entire composition range. The obtained results were compared with experimental values, yielding an average standard deviation of lower than 0.02 and an average relative deviation of less than 5%.

(2) The VLE phase diagrams (T–x–y and p–x–y) of Ag−Cu and Ag−Sb binary alloys were predicted based on M-MIVM and vacuum theory. These diagrams can offer valuable insights into the vacuum separation process. For instance, the Ag−Sb binary alloy under 10 Pa could achieve Sb content of greater than 99.99% in the vapor phase at temperatures below 1025.14 K.

(3) The findings reveal that the effective separation of the Ag−Cu binary alloy can be attained via the vacuum method, whereby Ag is primarily distributed in the vapor phase. In turn, the effective separation for the Ag−Sb binary alloy can be achieved through the multi-step distillation, and Sb is predominantly distributed in the vapor phase.

(4) The experimental and predicted VLE values for Ag−Cu and Ag−Sb binary alloys follow the same trends with temperature and exhibit minor deviations. Consequently, these theoretical VLE data can be used to estimate the degree of separation and product composition quantitatively. For example, the Ag−Sb binary alloy with a mass of 100 g containing 50% Ag should theoretically yield a distillate of 50.80 g and a residue of 49.20 g at 1273 K and 10 Pa.

CRediT authorship contribution statement

Qing-song LI: Data curation, Writing – Original draft, Conceptualization; **Bin YANG:** Supervision, Resources, Methodology; **Yang TIAN:** Formal analysis, Writing – Review & editing, Software; **Bao-qiang XU:** Funding acquisition, Visualization, Conceptualization; **Wen-long JIANG:** Formal analysis, Project administration; **Yuan GAO:** Software, Data curation; **Zong-kui JIANG:** Methodology, Validation.

Declaration of competing interest

The authors declare that they have no known competing financial interests or personal relationships that could have appeared to influence the work reported in this paper.

Acknowledgments

This work was financially supported by the National Natural Science Foundation of China (No. 52274352).

References

[1] RAUTIO T, HAMADA A, KUMPULA J, JÄRVENPÄÄ A, ALLAM T. Enhancement of electrical conductivity and corrosion resistance by silver shell−copper core coating of additively manufactured AlSi10Mg alloy [J]. Surface and Coatings Technology, 2020, 403: 126426.

[2] SONG Li, WANG Ying, YANG Ming, HUANG Yan. Investigation on stability of silver nanoparticles with different ligands [J]. Journal of Nanoparticle Research, 2023, 25(12): 255.

[3] WANG Shuang-ping, ZHAO Jin-yang, XU Bao-qiang, KONG Ling-xin, JIANG Wen-long, YANG Bin. Theoretical research on vacuum separation of Au−Ag alloy [J]. Transactions of Nonferrous Metals Society of China, 2022, 32(8): 2719−2726.

[4] GOULD I R, LENHARD J R, MUENTER A A, GODLESKI S A, FARID S. Two-electron sensitization: A new concept for silver halide photography [J]. Journal of the American Chemical Society, 2000, 122(48): 11934−11943.

[5] YANG Cai, LEI Xiao-jie, SHI Bai-sheng. Spillovers among China's precious and industrial metals markets: Evidence from higher moments and jumps [J]. Transactions of Nonferrous Metals Society of China, 2022, 32(4): 1362−1384.

[6] YU Qin-qin, MENG Kai-ning, GUO Juan-ling. Research on innovative application of silver material in modern jewelry design [J]. MATEC Web of Conferences, 2018, 176: 02013.

[7] ZHAN Hai-jiao, GUO Jia-yu, SHEN Jia-li, WANG Xiao-rong, FAN Zhong-hua, GUO Bing, LIU Wei, SHEN Hang-yan. Synthesis of silver flakes and their application as conductive filler for low-curing-temperature silver pastes [J]. Journal of Electronic Materials, 2019, 48(5): 2745−2753.

[8] LAI Yao-bin, ZHU Si-tian, LI Jian, ZHANG Hui, QI Tao. One-step synthesis of micro-sized flake silver particles as electrically conductive adhesive fillers in printed electronics [J]. Journal of Industrial and Engineering Chemistry, 2023, 121: 77−91.

[9] WANG Ye-ming, ZHANG Chao-qun, LI Shi-zhe, LIU Li-hui, FENG Xiao-dong, LIU Gang. Silver-catalyzed and silver-promoted reactions of isocyanides [J]. European Journal of Organic Chemistry, 2023, 26(23): e202300323.

[10] ZHANG Lin, ZHANG Hong. Silver halide-based nanomaterials in biomedical applications and biosensing diagnostics [J]. Nanoscale Research Letters, 2022, 17(1): 114.

[11] USGS. https://www.usgs.gov/.

[12] XU Zhi-peng, JIA Li-li, HE Zhi-qiang, GUO Xue-yi, TIAN Qing-hua. A review of preparing high-purity metals by vacuum distillation [J]. Transactions of Nonferrous Metals Society of China, 2024, 34(5): 1634−1654.

[13] YANG Bin, HUANG Da-xin, LIU Da-chun, ZHA Guo-zheng, JIANG Wen-long, KONG Xiang-feng. Research and industrial application of a vacuum separation technique for recovering valuable metals from copper dross [J]. Separation and Purification Technology, 2020, 236: 116309.

[14] HUANG Da-xin, JIANG Wen-long, XU Bao-qiang, ZHA Guo-zheng, YANG Bin. Purification of metallurgical-grade crude tellurium based on viscous distillation and gas-phase separation [J]. Transactions of Nonferrous Metals Society of China, 2024, 34(3): 1037−1048.

[15] GUO Xin-yu, ZHOU Yi, ZHA Guo-zheng, JIANG Wen-long, YANG Bin, MA Wen-hui. A novel method for extracting metal Ag and Cu from high value-added secondary resources by vacuum distillation [J]. Separation and Purification Technology, 2020, 242: 116787.

[16] YI Jia-fei, ZHA Guo-zheng, HUANG Da-xin, KONG Xiang-feng, YANG Bin, LIU Da-chun, XU Bao-qiang. Effective separation and recovery of valuable metals from high value-added lead anode slime by sustainable vacuum distillation [J]. Journal of Cleaner Production, 2021, 319: 128731.

[17] WANG Ya-nan, CHEN Liang-liang, KONG Ling-xin, YANG Bin. Simulation prediction and experimental study of phase equilibria of Bi−Sb and Bi−Sb−Cd alloys in vacuum distillation [J]. Vacuum, 2023, 213: 112032.

[18] FROST M, von SOLMS N, RICHON D, KONTOGEORGIS G M. Measurement of vapor−liquid−liquid phase equilibrium: Equipment and results [J]. Fluid Phase Equilibria, 2015, 405: 88−95.

[19] NAN Chang-Bin, XIONG Heng, XU Bao-qiang, YANG Bin, LIU Da-Chun, YANG Hong-Wei. Measurement and modeling of phase equilibria for Sb−Sn and Bi−Sb−Sn alloys in vacuum distillation [J]. Fluid Phase Equilibria, 2017, 442: 62−67.

[20] YANG Hong-Wei, XU Bao-qiang, YANG Bin, MA Wen-hui, TAO Dong-ping. Calculation of phase equilibrium in vacuum distillation by molecular interaction volume model [J]. Fluid Phase Equilibria, 2012, 314: 78−81.

[21] KONG Ling-xin, YANG Bin, XU Bao-qiang, LI Yi-fu, LI Liang, LIU Da-chun, DAI Yong-nian. Application of molecular interaction volume model in separation of Pb−Sn−Sb ternary alloy by vacuum distillation [J]. Transactions of Nonferrous Metals Society of China, 2013, 23(8): 2408−2415.

[22] YOU Yan-jun, KONG Ling-xin, XU Jun-jie, LIU Gang-gang, YANG Bin. Calculation of evaporation rates of all components in Ag−Pb−Sn ternary alloy in vacuum distillation using modified molecular interaction volume model [J]. Materials Research Express, 2019, 8(7): 076509.

[23] PANG Jian, WU Hai, KONG Ling-xin, XU Bao-qiang, XU Jun-jie, YANG Bin. Clean and efficient recovery of In−Sn and In−Sn−Bi lead-free brazing materials by vacuum volatilization and thermodynamic modeling [J]. Vacuum, 2023, 214: 112172.

[24] DAI Heng, TAO Dong-ping. Application of the modified molecular interaction volume model (M-MIVM) to vapor-liquid phase equilibrium of binary alloys in vacuum distillation [J]. Vacuum, 2019, 163: 342−351.

[25] YOU Yan-jun, KONG Ling-xin, XU Jun-jie, XU Bao-qiang, LIU Gang-gang, YANG Bin. Prediction of activities of all components in Sn−Ag−Cu and Sn−Ag−Cu−Zn lead-free solders using modified molecular interaction volume model [J]. Results in Chemistry, 2021, 3: 100143.

[26] YOU Yan-jun, XU Jun-jie, KONG Ling-xin, XU Bao-qiang, YANG Bin. Calculation of vapor-liquid equilibrium of binary precious metal alloys using modified molecular interaction volume model [J]. Materials Research Express, 2021, 8(9): 096508.

[27] HULTGREN R, DESAI P D, HAWKINS D T, GEISER M, KELLEY K K. Selected values of the thermodynamic properties of binary alloys [M]. Metals Park, OH: American Society of Metals, 1973.
[28] SGTE. Phase equilibria, crystallographic and termodynamic data of binary alloys [M]//Landolt-börnstein-Group IV Physical Chemistry. Berlin: Springer-Verlag, 2002.
[29] GIERLOTKA W, JENDRZEJCZYK-HANDZLIK D, FITZNER K, HANDZLIK P. On the ternary Ag−Cu−Ga system: Electromotive force measurement and thermodynamic modeling [J]. Journal of Alloys and Compounds, 2015, 646: 1023−1031.
[30] ZHAO Su, LI Jin-fu, LIU Li, ZHOU Yao-he. Solidification of undercooled Ag−Cu eutectic alloy with the Sb addition [J]. Journal of Alloys and Compounds, 2009, 478(1/2): 252−256.
[31] DAI Heng, TAO Dong-ping. Application of the molecular interaction volume model (MIVM) and its modified form to organic vapor-liquid equilibria [J]. Fluid Phase Equilibria, 2019, 484: 74−81.
[32] TAO Dong-ping. Prediction of the coordination numbers of liquid metals [J]. Metallurgical and Materials Transactions A, 2005, 36(12): 3495−3497.
[33] DAI Yong-nian, YANG Bin. Vacuum metallurgy of nonferrous metal materials [M]. Beijing: Metallurgical Industry Press, 2000. (in Chinese)
[34] PANG Jian, WU Hai, KONG Ling-xin, XU Jun-jie, XU Bao-qiang, YANG Bin. Vacuum distillation: A sustainable separation and purification approach for extracting valuable metals from In−Zn, In−Sn, and In−Sn−Zn waste alloys [J]. Separation and Purification Technology, 2024, 330: 125166.
[35] JACKSON P L, WILSAK R A. Thermodynamic consistency tests based on the Gibbs-Duhem equation applied to isothermal, binary vapor-liquid equilibrium data: data evaluation and model testing [J]. Fluid Phase Equilibria, 1995, 103(2): 155−197.
[36] Nan Chang-bin. Experimental study of gas-liquid phase equilibrium in vacuum distillation of tin-based alloys [D]. Kunming University of Science and Technology, 2017. (in Chinese)
[37] WILLIAMSON J C. Liquid−liquid demonstrations: Phase equilibria and the lever rule [J]. Journal of Chemical Education, 2021, 98(7): 2356−2363.

银铜和银锑二元合金真空蒸馏相平衡的模拟预测与实验研究

李青松[1,2,3]，杨 斌[1,2,3,4]，田 阳[1,2,3,4]，徐宝强[1,2,3,4]，蒋文龙[1,2,3,4]，高 源[1,2,3]，姜宗魁[1,2,3]

1. 昆明理工大学 云南省有色金属真空冶金重点实验室，昆明 650093；
2. 昆明理工大学 真空冶金国家工程研究中心，昆明 650093；
3. 昆明理工大学 冶金与能源工程学院，昆明 650093；
4. 昆明理工大学 省部共建复杂有色金属资源清洁利用国家重点实验室，昆明 650093

摘 要：采用修正分子相互作用体积模型(M-MIVM)计算银铜和银锑二元合金的活度预测值及其与实验值的偏差；利用 M-MIVM 和真空理论相结合绘制了其理论气液相平衡相图(T–x–y 和 p–x–y)；开展了银铜合金在 1500~1560 K、10~15 Pa 条件下和银锑合金在 950~1350 K、10 Pa 条件下的气液相平衡(VLE)实验。结果表明，活度的平均相对偏差和平均标准偏差分别低于 5%和 0.02。VLE 的理论和实验结果对比发现，T–x–y 图中的理论数据与实验数据具有良好的一致性。因此，VLE 相图可以为银铜和银锑二元合金的真空分离实验和工业生产提供指导。

关键词：银铜二元合金；银锑二元合金；修正分子相互作用体积模型(M-MIVM)；气液相平衡；活度

(Edited by Xiang-qun LI)